Published in final edited form as:
Mol Imaging Biol. 2012 August ; 14(4): 500–508. doi:10.1007/s11307-011-0512-4.

Integrin $\alpha_v\beta_3$ as a PET Imaging Biomarker for Osteoclast Number in Mouse Models of Negative and Positive Osteoclast Regulation

Alexander Zheleznyak[1], **Thaddeus J. Wadas**[1,6], **Christopher D. Sherman**[1], **Jessica M. Wilson**[1], **Paul J. Kostenuik**[5], **Katherine N. Weilbaecher**[2], and **Carolyn J. Anderson**[1,3,4,7]

[1]Mallinckrodt Institute of Radiology, Washington University School of Medicine, St. Louis, MO, USA

[2]Department of Medicine, Washington University School of Medicine, St. Louis, MO, USA

[3]Department of Biochemistry & Molecular Biophysics, Washington University School of Medicine, St. Louis, MO, USA

[4]Department of Chemistry, Washington University, St. Louis, MO, USA

[5]Department of Metabolic Disorders, Amgen, Inc., Thousand Oaks, CA, USA

Abstract

Purpose—The goal of this study was to determine the specificity of ^{64}Cu-CB-TE2A-c(RGDyK) (^{64}Cu-RGD) for osteoclast-related diseases, such as Paget's disease or rheumatoid arthritis.

Procedures—C57BL/6 mice were treated systemically with osteoprotegerin (OPG) for 15 days or RANKL for 11 days to suppress and stimulate osteoclastogenesis, respectively. The mice were then imaged by positron emission tomography/computed tomography using ^{64}Cu-RGD, followed by determination of serum TRAP5b and bone histology. Standard uptake values were determined to quantify ^{64}Cu-RGD in bones and other tissues.

Results—Mice treated with OPG showed decreased bone uptake of ^{64}Cu-RGD at 1, 2, and 24 h post-injection of the tracer ($p<0.01$ for all time points) compared to vehicle controls, which correlated with a post-treatment decrease in serum TRAP5b. In contrast, mice treated with RANKL showed significantly increased bone uptake at 2 h post-injection of ^{64}Cu-RGD ($p<0.05$) compared to the vehicle control group, corresponding to increased serum TRAP5b and OC numbers as determined by bone histology.

Conclusions—These data demonstrate that ^{64}Cu-RGD localizes to areas in bone with increased osteoclast numbers and support the use of ^{64}Cu-RGD as an imaging biomarker for osteoclast number that could be used to monitor osteoclast-related pathologies and their treatments.

Correspondence to: Carolyn J. Anderson; andersoncj@upmc.edu.
[6]Current Address: Department of Cancer Biology, Wake Forest University, Winston-Salem, NC, USA
[7]Current Address: Department of Radiology, University of Pittsburgh, 100 Technology Drive; Suite 452, Pittsburgh, PA 15219, USA

Conflict of Interest. Dr. Anderson received partial support for the research presented here from Amgen, Inc. Dr. Kostenuik is an employee of Amgen, Inc.

Keywords

PET imaging; Copper-64; Osteoclast regulation; Integrin

Introduction

Bone diseases are often accompanied by an increased number of osteoclasts, and osteolytic bone metastases are a significant cause of morbidity in many types of cancer. Increased osteoclastogenesis promotes osteolytic activity and bone loss, which can result in pain, pathologic fracture, spinal cord compression, and hypercalcemia [1, 2]. It has been reported that 30–85% of patients with metastatic breast cancer will develop metastatic bone lesions, which can be osteolytic, osteoblastic, or mixed in nature [2]. Importantly, micro-metastases are often associated with poor outcome in patients with small node-negative primary tumors [3].

Osteoclasts are multinucleated cells of the macrophage/monocyte lineage that uniquely function as the bone resorptive cells. Osteoclastogenesis is regulated by two cytokines from the tumor necrosis factor family of proteins: osteoprotegerin (OPG) and receptor activator of nuclear factor κB ligand (RANKL). Both cytokines are produced by the osteoblasts and influence bone remodeling by modulating the number of active osteoclasts. RANKL, through its interaction with RANK receptor, directs bone marrow macrophages to differentiate into active osteoclasts, while OPG, a decoy receptor for RANKL, negatively regulates RANKL's effect on macrophages [4]. In this context, the RANKL–OPG system provides a convenient way of manipulating the number of osteoclasts *in vivo* to model osteoclastogenesis.

Alpha v beta 3 ($\alpha_V\beta_3$) is the major integrin expressed by mature, active osteoclasts [5]. Integrin $\alpha_V\beta_3$ is a heterodimeric transmembrane glycoprotein which has been shown to play an important role in angiogenesis and tumor metastasis to the bone [6]. Consequently, $\alpha_V\beta_3$ has been evaluated as a potential site for therapeutic intervention. In addition, $\alpha_V\beta_3$ is the most abundant integrin on the surface of the osteoclast which makes it a useful imaging target for diseases resulting in increased osteoclast numbers [5].

Imaging bone pathology has been a challenging undertaking. Both ^{99m}Tc-methyl diphosphonate (MDP) imaging with gamma scintigraphy and 2-deoxy-2-[^{18} F]fluoro-D-glucose (^{18}F-FDG) positron emission tomography (PET) have been utilized to detect and monitor metastatic bone disease [7-10]. However, ^{99m}Tc-MDP and similar radiopharmaceuticals preferentially identify osteoblastic lesions [8]. ^{18}F-FDG uptake is increased in cells and tissues undergoing rapid division, growth, and inflammatory response. These processes are transient and are not necessarily tumor-specific [7, 11, 12]. Du *et al*. showed that ^{18}F-FDG was taken up in both osteolytic and osteoblastic lesions, with SUV_{max} values correlating to the size of the tumor rather than whether the lesion was osteolytic or osteoblastic [10]. Consequently, these methods have shown poor effectiveness in imaging elevated numbers of osteoclasts associated with neoplastic metastatic activity in the bone. Imaging methods which rely on the bone density, such as x-ray or computed tomography (CT), are effective only when the bone tissue is significantly resorbed [9]. It is therefore

clinically relevant to develop a method for imaging osteoclasts, which would be sensitive enough to detect the increases in cell numbers associated with osteolytic metastases.

Previous studies have shown that the Arg-Gly-Asp tri-peptide (RGD) binds to $\alpha_v\beta_3$ with high affinity [13, 14]. Several linear and cyclic RGD-based ligands have been analyzed for their effectiveness at $\alpha_v\beta_3$ targeting [13]. These small molecules have better tumor-penetrating capacity than the much larger protein-based tracers, such as antibodies. Also, there is less chance of them being detected by the reticulo-endothelial system and eliciting an immune response.

There are reports in the literature on the development and human studies of ^{18}F-labeled RGD agents for imaging tumor angiogenesis, specifically ^{18}F-galacto-RGD [15-19]. This agent has been investigated in human PET imaging trials in patients with breast, melanoma, head and neck cancer and glioma, and has demonstrated specific imaging of the $\alpha_v\beta_3$ integrin both in tumors and angiogenic blood vessels.

We reported on a cyclized version of RGD, c(RGDyK), conjugated to the cross-bridged chelator CB-TE2A (4,11-bis (carboxymethyl)-1,4,8,11-tetraazabicyclo[6.6.2]hexadecane) for radiolabeling with ^{64}Cu ($t_{1/2}$ =12.7 h, β^+ =17.4%, $E_{\beta+max}$ = 656 keV; β^- =39%, $E_{\beta-max}$ =573 keV) (Fig. 1), and showed that this agent demonstrated good *in vivo* stability and clearance from blood and liver [14]. Unlike ^{18}F, ^{64}Cu has a half-life compatible with overnight shipping protocols and can be produced at a distant cyclotron site with high specific activity, making ^{64}Cu-CB-TE2A-c(RGDyK) (or ^{64}Cu-RGD) an attractive radiopharmaceutical. This compound has been shown to be highly effective as an osteoclast imaging agent *in vivo* in a pharmacological mouse model of direct administration of parathyroid-hormone into the calvarium [14] as well as in a mouse model of osteolytic bone metastasis [20]. As the ^{64}Culabeled RGD agent has already demonstrated uptake in osteoclasts, here, we used ^{64}Cu-RGD to visualize changes in osteoclast number in response to systemically administered OPG and RANKL. An imaging agent targeting osteoclasts, which are upregulated in osteolytic lesions, may facilitate earlier follow-up in patients with osteolytic or mixed bone metastases. Therapies for bone metastases include bisphosphonates and the anti-RANKL antibody, denosumab, which inhibit the production of osteoclasts. The ability to image increased numbers of osteoclasts may also have significance for imaging and monitoring therapy of osteoporosis and rheumatoid arthritis (RA).

Experimental

Methods and Materials

OPG-Fc and RANKL were provided by Amgen, Inc. All experiments involving the use of radioactive materials at Washington University is conducted under the authorization of the Radiation Safety Committee in accordance with the University's Nuclear Regulatory Commission license. Copper-64 (half-life, 12.7 h; β^+ 17.8%; $E_{\beta+max}$, 656 keV; β^- 38.4%; $E_{\beta-max}$, 573 keV) was produced on a biomedical cyclotron (CS-15; Cyclotron Corp.) at Washington University School of Medicine. CB-TE2A-c(RGDyK) was prepared as previously described [14]. All chemicals were purchased from Sigma-Aldrich (St. Louis, MO, USA), unless otherwise specified, and solutions were prepared using ultrapure water

(18 MΩ-cm resistivity). Radiochemistry reaction progress and purity were monitored by analytical reversed-phase high-performance liquid chromatography (HPLC), which was performed on a Waters 600E chromatography system (Milford, MA, USA) with a Waters 991 photodiode array detector and an Ortec Model 661 radioactivity detector (EG&G Instruments, Oak Ridge, TN, USA). An Altima C18 Rocket® column was employed with a gradient that changes from 0.1% TFA in water to 30:70 0.1%TFA/water:0.1%TFA/CH_3CN over the course of 5 min. In addition, radio-TLC was conducted on a Bioscan AR 2000 radio-TLC scanner equipped with a 10% methane/argon gas supply and a PC interface running Winscan v.3 analysis software. C-18 plates were employed using an eluent mixture of 3:7 10% NH_4OAc/MeOH, and the complex $^{64}Cu(OAc)_2$ as a standard control. Radioactive samples were counted using a Beckman 8000 (Franklin Lakes, NJ, USA) automated well-type gamma-counter. PET and CT data were acquired using either a microPET Focus 120 or a microPET Focus 220 and a microCAT II system, respectively (Siemens Medical Solutions, Knoxville, TN, USA).

Animal Handling

Male C57BL/6 mice (5 weeks) were purchased from Charles River Laboratories, (Wilmington, MA, USA) and housed under pathogen-free conditions in an approved facility according to the guidelines of the Division of Comparative Medicine and the Animal Studies Committee of Washington University School of Medicine.

Radiochemistry

The complexation of ^{64}Cu to CB-TE2A-c(RGDyK) was achieved by reacting 2 μg (1.3×10^{-3} μmol) of CB-TE2A-c (RGDyK), 118 μL solution of 0.1 M NH_4OAc (pH=8.0) and 37 MBq (1,000 μCi) of $^{64}CuCl_2$ in 0.1 N HCl for 1.5 h at 95°C. If needed, the reaction was further purified using a previously published method [21]. Purity was greater than 95% based upon radio-HPLC and radio-TLC analysis and the specific activities ranged from (11–37 MBq (300–1,000 μCi)/μg).

OPG and RANKL Treatment Protocol

Male C57BL/6 mice (~23 g) were treated with OPG in doses of 0.2, 1.0, and 5.0 mg/kg dose in 100-μL saline twice a week for 2 weeks subcutaneously in the nape of the neck while under brief Isoflurane anesthesia. Control groups received saline according to the same schedule. Male C57BL/6 mice (~23 g) were treated with RANKL in doses of 0.3 or 0.1 mg/kg (dose diluted in 50-μL saline) twice a day for 10 days subcutaneously in the nape of the neck while under brief isoflurane anesthesia.

Biodistribution

Biodistribution studies were conducted according to previously published protocols [14]. Briefly, on day 15(OPG) or day 11 (RANKL), treated and control mice were injected (IV, tail, heat, and restraint) with 20 μCi ^{64}Cu-RGD. Animals were sacrificed at selected time points post-injection (p.i.), organs of interest were removed, weighed, and counted. The percent-injected dose per gram (%ID/gram) and percent-injected dose per organ (%ID/organ) were calculated by comparison to a weighed, counted standard.

Blood Collection and Serum Tartrate-Resistant Acid Phosphatase (TRAP5b) Analysis

Blood samples from RANKL and OPG treated and control cohorts were collected by submandibular venous puncture before the biodistribution study or at the time of sacrifice. Serum was obtained by centrifuging the blood at 10,000 rpm for 5 min at 4°C in the serum separator tubes (Becton Dickinson; Franklin Lakes, NJ, USA) and stored at −20°C until use. A solid-phase immunoassay was used to measure osteoclastic TRAP5b activity. The MouseTRAP–immunoassay kit was purchased from SBA Science/IDS Inc. (Fountain Hills, AZ, USA), and assays were performed according to the manufacturer's instructions.

Small Animal PET/CT Imaging

Male C57BL/6 mice (~23 g) were treated with RANKL in doses of 0.3 mg/kg (dose diluted in 50-μL saline) twice a day for 10 days. On day 11, treated and control mice (n=4 for each group) were injected with 300 μCi ^{64}Cu-RGD (5.6– 11.1 MBq) and imaged using small animal PET/CT 2, 4, and 24 h p.i., Co-registered images were re-constructed using the *maximum a posteriori* (MAP) algorithm [22], and regions of interest (ROI) were determined from the co-registered PET/ CT images with AMIDE imaging software [23]. Standard uptake values (SUV) were determined as [(nanocurie per milliliter) × (animal weight (grams))/injected dose (nanocurie)]. Blood, lung, liver, muscle, kidney, spleen, leg bones, and tail were collected and counted for radioactivity for a post-imaging biodistribution.

Histology

After sacrifice from the biodistribution and the small animal imaging studies, the femur and tibia were removed, fixed in 10% formalin for 48 h, decalcified in a 14% EDTA solution replacing the buffer three times over a period of 14 days, embedded in paraffin, sectioned longitudinally at a thickness of 20 μm. Sections were stained with hematoxylin and eosin, and counterstained with TRAP to identify osteoclasts. Images were visualized under a Nikon Eclipse TE300 microscope equipped with a Plan Fluor 20/0.45 objective lens (Nikon) and MagnaFire digital charge-coupled device camera according to a standard protocol using the Osteomeasure Analysis System software (Osteometrics). The field of analysis included the entire tibia and femur, including cortical and trabecular bone. TRAP-positive osteoclasts were enumerated and divided by total bone tissue area.

Statistical Analysis

All data are presented as mean ±SD. For statistical classification, a Student's t test (two-tailed, unpaired) was used to compare individual datasets. All statistical analyses were performed using PRISM software (GraphPad). P values less than 0.05 were considered significant.

Results

Decreased ^{64}Cu-CB-TE2A-c(RGDyK) PET Uptake in Bones with Reduced Osteoclast Numbers After OPG-Fc Administration

Biodistribution studies after administration of PET imaging agent ^{64}Cu-RGD (Fig. 1) were performed on animals receiving a high (5 mg/kg twice a week for 2 weeks) dose of OPG and

vehicle controls. Organs were harvested at appropriate times post-tracer administration and serum was collected for the TRAP5b level analysis. Although tracer accumulation in non-skeletal tissues of animals treated with 5 mg/mL of OPG-Fc was indistinguishable from vehicle control animals (Fig. 2a), tracer accumulation in the leg bones of these animals was observed to be significantly less at 1 h post injection when compared to the control animals (OPG vs. saline;%ID/g, p value, 0.52 ±0.05 vs. 0.63 ±0.03, $p<0.005$). Additionally, radiotracer uptake at 2 h p.i. (0.35 ± 0.06 vs. 0.43 ±0.04, $p<0.005$) and 24 h p.i. (0.26 ±0.04 vs. 0.32 ±0.03, $p<0.05$) was also significantly less in the leg bones of treated animals (Fig. 2b). Serum TRAP5b is used as a measure of osteoclastogenesis and correlates with osteoclast number in bone [24] As expected, mice treated with 5 mg/kg OPG-Fc twice a week for 2 weeks had significantly decreased levels of serum TRAP5b (0.39±0.04 U/L) when compared to either the control mice (2.4±0.19 U/L) or mice prior to treatment (2.0±0.20 U/L) (Fig. 2c). Taken together, these data demonstrate that ^{64}Cu-CB-TE2A-c(RGDyK) in bone was significantly lower in OPG-treated mice with decreased osteoclasts (as measured by serum TRAP5b and histology) compared to vehicle-treated mice.

Increased ^{64}Cu-CB-TE2A-c(RGDyK) Uptake in Bones with Increased Osteoclast Numbers After RANKL Administration

Biodistribution of ^{64}Cu-RGD and serum TRAP5b levels were performed in mice administered 0.3 mg/kg RANKL twice a day for 10 days or vehicle control. After 10 days, mice injected with ^{64}Cu-RGD or saline were sacrificed at 1, 2, and 24 h post tracer injection and tracer biodistribution measured in bones and organs. Serum was collected for TRAP5b level determination.

The non-skeletal tissue biodistribution of ^{64}Cu-RGD assessed at 2 h after injection of the tracer did not vary significantly between the control and treated animals (Fig. 3a). In contrast, the leg bones of mice treated with 0.3 mg/kg of RANKL showed an increase in the uptake of ^{64}Cu-RGD when compared to the bones from animals treated with saline at 1 and 2 h after injection of the tracer (Fig. 3a). At 1 h post tracer injection, the bones from RANKL-treated animals retained 4.3 times more activity than the control mice, 3.8 vs. 0.88%ID/g. This differential increased to 7.5-fold at 2 h post tracer injection, 6.4 vs. 0.85%ID/g. The serum level of TRAP5b increased in RANKL-treated animals at both the 1- and 2-h time points (Fig. 3b). ^{64}Cu-RGD uptake in the bone is depicted together in Bones with serum TRAP5b data (Fig. 3b).

Small Animal PET/CT Imaging Demonstrated Increased Tracer Uptake in Leg Bones of Animals Treated with RANKL

In experiments separate from the biodistribution studies, small animal PET/CT imaging was performed to evaluate the ability of ^{64}Cu-RGD to accurately image and quantify osteoclast number in living animals treated with RANKL prior to imaging. A maximal intensity projection of a representative PET/CT image is shown in Fig. 4a. Increased uptake of the radiopharmaceutical was clearly visible in the femorotibial juncture of RANKL-treated animals when compared to animals treated with saline. SUVs obtained for RANKL-treated mice were 3.7 times higher than the SUV obtained from the control animals at 2 h after the tracer administration, with mean values being 0.12 (SE=0.02) and 0.03 (SE=0.02),

respectively (Fig. 4b), and correlated well with serum TRAP5b results, which indicated a significant 1.6-fold increase in RANKL-treated groups when compare to the control cohort (Fig. 4c). SUVs obtained from scans performed 4 and 24 h after tracer administration did not show significant differences between the treated and the control groups, suggesting that the tracer was cleared from the bones at these later time points. After imaging, mice were sacrificed, leg bones were excised, de-calcified, stained for TRAP, and analyzed by histomorphometry. The microscopic evidence of the significant increase in osteoclast numbers can be seen in Fig. 5. Figure 5a shows a femur from a RANKL-treated animal, demonstrating an increase in TRAP+ cells when compared to the femoral bone from a control animal, which is presented in Fig. 5b. Interestingly, bones from RANKL-treated animals were almost completely devoid of trabecular bone with the TRAP+ cells localized to the endosteal area. Histomorphometric analysis applied to the TRAP-stained sections demonstrated a 1.6-fold increase in the number of TRAP+ cells in bones of RANKL-treated animals (Fig. 5d), thus establishing the correlative relationship between osteoclast numbers and ^{64}Cu-RGD tracer uptake measured by small animal PET (Fig. 5e).

Conversely, the femur from an OPG-Fc-treated mouse obtained from a biodistribution study exhibited a distinctive osteopetrotic phenotype characterized by an extended growth plate with abundant trabecular bone and severely decreased osteoclastogenesis (Fig. 5c). Taken together, these data demonstrate that ^{64}Cu-RGD and small animal PET/CT was sensitive enough to detect increased uptake in bones of living mice with increased osteoclast number and decreased bone uptake in bones of mice with decreased OC number.

Discussion

In this report, we demonstrate the efficacy of ^{64}Cu-RGD radiotracer as a PET imaging agent of osteoclasts with potential applications in prognostication and staging of metastatic bone disease, or other osteoclast-related pathologies such as osteoporosis or RA, as well as for monitoring anti-osteoclast therapies. Bone tropism is a common characteristic of cancers originating in lung, breast, prostate, and thyroid gland [25, 26]. Metastatic complications of these malignancies are predominantly of an osteolytic etiology, and pathologically active osteoclastogenesis has been shown to be a valuable indicator for both diagnosis and therapy. For example, Roato *et al*. identified increased osteoclastogenesis as a prognosticative factor in non-small cell lung cancer (NSCLC) [27]. Bone metastasis from prostate cancer can create osteolytic, osteoblastic or mixed (lytic/blastic) lesions, and an osteoclast imaging modality capable of identifying patients with lytic or mixed lesions might help to tailor anti-resorptive therapies to those most likely to benefit from osteoclast inhibition. Osteolytic bone destruction is also a major factor in the pathophysiology of RA. In this case, a number of developing therapies act to restore the osteoclast/ osteoblast homeostasis [28] RA and NSCLC could clearly benefit from an assessment of *in situ* osteoclastogenesis.

^{64}Cu-RGD incorporates the cyclic c(RGDyK) moiety, a high-affinity ligand for $\alpha_V\beta_3$, which is characteristically overexpressed on active osteoclasts [6] Numerous studies have established the $\alpha_V\beta_3$ integrin as an attractive target for molecular imaging of various pathologies [29-31]. Sprague *et al*. showed that locally induced osteoclastogenesis could be imaged with ^{64}Cu-RGD and PET [14]. This study also demonstrated the specificity of ^{64}Cu-

RGD tracer using Western blotting and unlabeled tracer blocking techniques. Wadas *et al*. demonstrated the effectiveness of ^{64}Cu-RGD and small animal PET/CT in a mouse model of HTLV-1 adult T-cell leukemia (Tax+ transgenic) [20]. The data presented here extend these findings to demonstrate that a systemic modulation of osteoclastogenesis can be effectively imaged by ^{64}Cu-RGD and small animal PET/CT. Biodistribution studies were conducted to monitor the ^{64}Cu-RGD uptake in target and non-target tissues after systemic administration of osteoclastogenesis modulating cytokines OPG-Fc and RANKL. When the number of osteoclasts was increased by treatment with 0.3 mg/kg RANKL, the leg bones of treated animals retained on the average 4 to 7.5 times more ^{64}Cu-RGD than the bones of control animals (Fig. 3), while the uptake of ^{64}Cu-RGD in bones of control mice did not vary to any significant degree at all measured time points. Concomitant increase of TRAP5b levels in sera obtained from the RANKL-treated animals was consistent with an increase in bone resorption. This positive relationship suggested that ^{64}Cu-RGD uptake reflected active osteolysis by the target cell population. Inhibition of osteoclastogenesis with 5 mg/kg OPG-Fc resulted in modest, but statistically significant decreases in ^{64}Cu-RGD uptake in the leg bones of treated animals at 1 and 24 h post injection (Fig. 2). Although this decrease in tracer uptake was statistically significant, it was only about 1.2-fold less than the uptake in a corresponding control. This differential uptake suggests that the sensitivity of PET imaging might not be sufficient enough to detect the inhibition of osteoclast activation. As the result, PET imaging studies were conducted only with RANKL-treated animals.

Sites of actively remodeling skeleton, such as upper and lower extremities and jaw bones, have been evaluated in previous studies that examined osteoclastogenesis [32-34]. Mouse leg bones were selected to study the imaging characteristics of ^{64}Cu-RGD for three reasons. Firstly, the leg bones are the sites of fairly active bone remodeling processes. Secondly, leg bones could be easily dissected and analyzed by both biodistribution and histomorphometry. Finally, leg bones are easy to evaluate in a post-imaging analysis, including the generation of ROI than such complex shapes as jaw bones. Small animal PET/CT imaging studies reflected the findings of the biodistribution experiments. When SUVs obtained from the PET images were analyzed, tracer accumulation in the target tissues of RANKL-treated animals was significantly higher 2 h after administration. The observed difference, about 3.7-fold, correlated well with previously reported data [14, 20] Histological analysis conducted on the bones of RANKL-treated animals confirmed the expected increase in osteoclast number, suggesting that the SUV differential is due to the enhanced osteoclastogenesis. SUVs obtained from scans performed 4 and 24 h after tracer administration did not show significant differences between the treated and the control groups, possibly due to the internalization and subsequent redistribution of the tracer throughout the reticuloendothelial system, as demonstrated by the uptake in liver and gut.

Although the data demonstrate clear correlations between pharmacological treatment, bone associated activity and osteoclast number, variability in the data is observed (Fig. 3), which may be associated with inter-mouse variation in response to the RANKL treatment regimen. Walsh *et al*. noted that that pharmacologic modulation leads to variable responses within a cohort of study animals [35]. This may be due in part to the microfractures caused by a significant influx of active osteoclasts resulting in loss of bone tissue during the extraction

associated with the biodistribution procedure. Furthermore, PET imaging and serum TRAP5b level assessment, modalities that do not involve potentially damaging post-mortem tissue extraction, demonstrate much less inter-experimental variability than the biodistribution modality. We anticipate that earlier time points after the initiation of RANKL injections would have yielded greater overall osteoclast numbers, fewer or no microfractures, and a potentially greater accumulation of tracer.

TRAP5b is a well-established marker for osteoclast number; however, it represents the contribution of not only osteoclasts, but also immature precursor cells [36]. These cells likely do not overexpress $\alpha_v\beta_3$ integrin and, therefore, will not be targeted by ^{64}Cu-RGD. For these reasons, a direct correlation between the serum levels of TRAP5b and the SUV obtained from the PET images is not established here; rather TRAP5b was used to independently demonstrate the effects of OPG and RANKL in our system. Additionally, TRAP5b is a system serum marker that will monitor the level of osteoclasts and precursors throughout the mouse skeleton, whereas in the biodistribution and imaging studies, only the knee joints were monitored for level of uptake of ^{64}Cu-RGD. In order to establish whether the tracer uptake in the bone reflects the number of mature osteoclasts, histomorphometry studies were conducted (Fig. 5d, e), which demonstrate a positive correlation between the number of mature osteoclasts and the tracer uptake in the bone.

Conclusion

This report describes the evaluation of ^{64}Cu-RGD as a biomarker for osteoclast number associated with increased osteoclastogenesis. We demonstrated that the uptake of this radiotracer accurately reflected both osteopetrotic and osteoporotic phenotypes in biodistribution studies supported by the serum TRAP5b levels. Small-animal PET studies supported by biodistribution and histological analyses demonstrated that ^{64}Cu-RGD was capable of imaging an increase in osteoclastogenesis typically associated with pathologically active bone resorption *in vivo*. Overall, these data establish ^{64}Cu-RGD as a potentially effective imaging agent for the detection of pathologies associated and accompanied by an increase in osteoclast number. Since ^{64}Cu-RGD targets the $\alpha_V\beta_3$ integrin, its use can also be extended to imaging of metastases formed by $\alpha_V\beta_3$-bearing tumors.

Acknowledgments

This research was funded by NIH grants NRSA F32 CA115148 (TJW), R01 CA097250 (KNW), and P01 CA100730 (KNW) as well as funding from Amgen, Inc.

References

1. Kakonen SM, Mundy GR. Mechanisms of osteolytic bone metastases in breast carcinoma. Cancer. 2003; 97:834–839. [PubMed: 12548583]
2. Mundy GR. Metastasis to bone: causes, consequences and theraputic opportunities. Nature Rev Cancer. 2002; 2:584–593. [PubMed: 12154351]
3. Braun S, Vogl FD, Naume B, et al. A pooled analysis of bone marrow micrometastasis in breast cancer. N Engl J Med. 2005; 353:793–802. [PubMed: 16120859]
4. Teitelbaum SL. Osteoclasts: what do they do and how do they do it? Am J Pathol. 2007; 170:427–435. [PubMed: 17255310]

5. Horton MA, Dorey EL, Nesbitt SA, et al. Modulation of vitronectin receptor-mediated osteoclast adhesion by arg-gly-asp peptide analogs: a structure-function analysis. J Bone Miner Res. 1993; 8:239–247. [PubMed: 7680185]
6. Horton MA. The alpha v beta 3 integrin “vitronectin receptor”. Int J Biochem Cell Biol. 1997; 29:721–725. [PubMed: 9251239]
7. Roodman GD. Mechanisms of bone lesions in multiple myeloma and lymphoma. Cancer. 1997; 80:1557–1563. [PubMed: 9362422]
8. Peterson JJ, Kransdorf MJ, O'Connor MI. Diagnosis of occult bone metastases: positron emission tomography. Clin Orthop Relat Res. 2003; 415S:S120–S128. [PubMed: 14600601]
9. Hamaoka T, Madewell JE, Podoloff DA, Hortobagyi GN, Ueno NT. Bone imaging in metastatic breast cancer. J Clin Oncol. 2004; 22:2942–2953. [PubMed: 15254062]
10. Du Y, Cullum I, Illidge TM, Ell PJ. Fusion of metabolic function and morphology: sequential [18f]fluorodeoxyglucose positron-emission tomography/computed tomography studies yield new insights into the natural history of bone metastases in breast cancer. J Clin Oncol. 2007; 25:3440–3447. [PubMed: 17592153]
11. Bjurberg M, Henriksson E, Brun E, et al. Early changes in 2-deoxy-2-[18f]fluoro-d-glucose metabolism in squamous-cell carcinoma during chemotherapy *in vivo* and *in vitro*. Cancer Biother Radiopharm. 2009; 24:327–332. [PubMed: 19538055]
12. Mortimer JE, Dehdashti F, Siegel BA, et al. Metabolic flare: indicator of hormone responsiveness in advanced breast cancer. J Clin Oncol. 2001; 19:2797–2803. [PubMed: 11387350]
13. Haubner R, Wester HJ, Reuning U, et al. Radiolabeled alpha(v) beta3 integrin antagonists: a new class of tracers for tumor targeting. J Nucl Med. 1999; 40:1061–1071. [PubMed: 10452325]
14. Sprague JE, Kitaura H, Zou W, et al. Noninvasive imaging of osteoclasts in parathyroid hormone-induced osteolysis using a 64cu-labeled rgd peptide. J Nucl Med. 2007; 48:311–318. [PubMed: 17268030]
15. Beer AJ, Haubner R, Goebel M, et al. Biodistribution and pharmacokinetics of the {alpha}v{beta}3-selective tracer 18f-galactorgd in cancer patients. J Nucl Med. 2005; 46:1333–1341. [PubMed: 16085591]
16. Beer AJ, Haubner R, Sarbia M, et al. Positron emission tomography using [18f]galacto-rgd identifies the level of integrin {alpha}v{beta}3 expression in man. Clin Cancer Res. 2006; 12:3942–3949. [PubMed: 16818691]
17. Beer AJ, Haubner R, Wolf I, et al. Pet-based human dosimetry of 18f-galacto-rgd, a new radiotracer for imaging alpha v beta3 expression. J Nucl Med. 2006; 47:763–769. [PubMed: 16644745]
18. Beer AJ, Schwaiger M. Imaging of integrin alphavbeta3 expression. Cancer Metastasis Rev. 2008; 27:631–644. [PubMed: 18523730]
19. Schnell O, Krebs B, Carlsen J, et al. Imaging of integrin alpha(v) beta(3) expression in patients with malignant glioma by [18f] galactorgd positron emission tomography. Neuro Oncol. 2009; 11:861–870. [PubMed: 19401596]
20. Wadas TJ, Deng H, Sprague JE, et al. Targeting the alphavbeta3 integrin for small-animal pet/ct of osteolytic bone metastases. J Nucl Med. 2009; 50:1873–1880. [PubMed: 19875645]
21. Wadas TJ, Anderson CJ. Radiolabeling of teta- and cb-te2a-conjugated peptides with copper-64. Nat Protoc. 2006; 1:3062–3068. [PubMed: 17406569]
22. Qi J, Leahy RM. Resolution and noise properties of map reconstruction for fully 3-d pet. IEEE Trans Med Imaging. 2000; 19:493–506. [PubMed: 11021692]
23. Loening AM, Gambhir SS. Amide: a free software tool for multimodality medical image analysis. Mol Imaging. 2003; 2:131–137. [PubMed: 14649056]
24. Shidara K, Inaba M, Okuno S, et al. Serum levels of trap5b, a new bone resorption marker unaffected by renal dysfunction, as a useful marker of cortical bone loss in hemodialysis patients. Calcif Tissue Int. 2008; 82:278–287. [PubMed: 18421493]
25. Kang Y. Breast cancer bone metastasis: molecular basis of tissue tropism. J Musculoskelet Neuronal Interact. 2004; 4:379–380. [PubMed: 15758269]
26. Wu Z, McRoberts KS, Theodorescu D. The role of pten in prostate cancer cell tropism to the bone micro-environment. Carcinogenesis. 2007; 28:1393–1400. [PubMed: 17347137]

27. Roato I, Gorassini E, Buffoni L, et al. Spontaneous osteoclasto-genesis is a predictive factor for bone metastases from non-small cell lung cancer. Lung Cancer. 2008; 61:109–116. [PubMed: 18061306]
28. Choi Y, Arron JR, Townsend MJ. Promising bone-related therapeutic targets for rheumatoid arthritis. Nat Rev Rheumatol. 2009; 5:543–548. [PubMed: 19798028]
29. Chen X, Hou Y, Tohme M, et al. Pegylated arg-gly-asp peptide: 64cu labeling and pet imaging of brain tumor alphavbeta3-integrin expression. J Nucl Med. 2004; 45:1776–1783. [PubMed: 15471848]
30. Haubner R, Bruchertseifer F, Bock M, et al. Synthesis and biological evaluation of a (99m)tc-labelled cyclic rgd peptide for imaging the alphavbeta3 expression. Nuklearmedizin. 2004; 43:26–32. [PubMed: 14978538]
31. Hsu AR, Chen X. Advances in anatomic, functional, and molecular imaging of angiogenesis. J Nucl Med. 2008; 49:511–514. [PubMed: 18375921]
32. Kyrgidis A, Triaridis S, Vahtsevanos K, Antoniades K. Osteonecrosis of the jaw and bisphosphonate use in breast cancer patients. Expert Rev Anticancer Ther. 2009; 9:1125–1134. [PubMed: 19671032]
33. Nakamura H, Hiraga T, Ninomiya T, et al. Involvement of cell-cell and cell-matrix interactions in bone destruction induced by metastatic MDA-MB-231 human breast cancer cells in nude mice. J Bone Miner Metab. 2008; 26:642–647. [PubMed: 18979165]
34. Pozzi S, Vallet S, Mukherjee S, et al. High-dose zoledronic acid impacts bone remodeling with effects on osteoblastic lineage and bone mechanical properties. Clin Cancer Res. 2009; 15:5829–5839. [PubMed: 19737962]
35. Walsh NC, Gravallese EM. Bone loss in inflammatory arthritis: mechanisms and treatment strategies. Curr Opin Rheumatol. 2004; 16:419–427. [PubMed: 15201606]
36. Lacey DL, Tan HL, Lu J, et al. Osteoprotegerin ligand modulates murine osteoclast survival in vitro and in vivo. Am J Pathol. 2000; 157:435–448. [PubMed: 10934148]

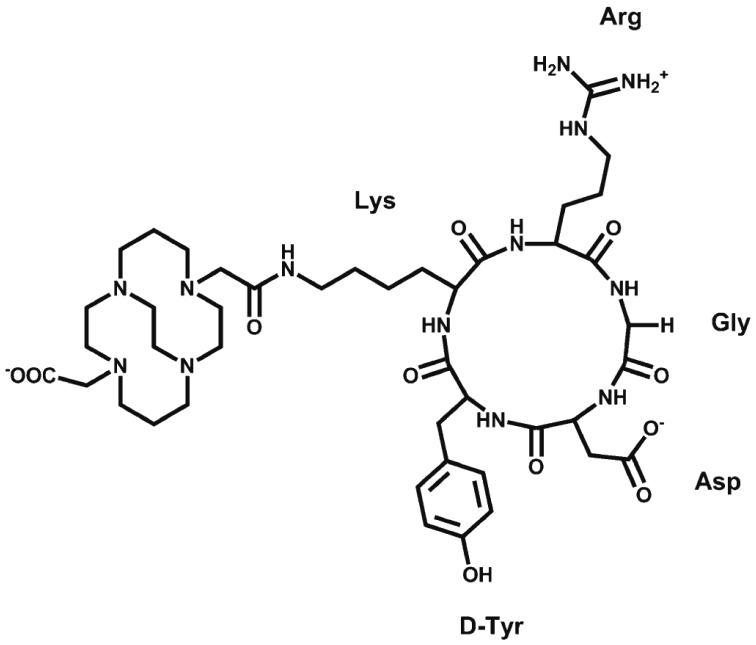

Fig. 1.
Structure of ^{64}Cu-CB-TE2A-c(RGDyK).

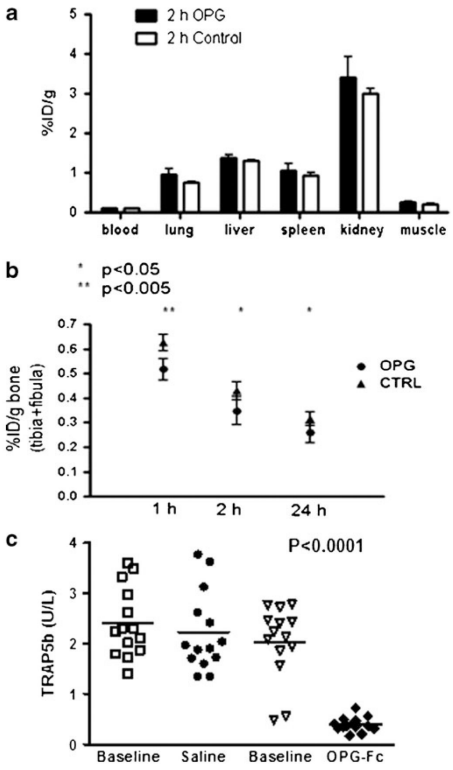

Fig. 2.

Decreased ^{64}Cu-RGD uptake in leg bones of animals treated with 5 mg/kg OPG-Fc. **a** ^{64}Cu-RGD retained in non-target organs of treated and control animals demonstrated no significant difference (2 h PI shown). **b** Statistically significant decrease in ^{64}Cu-RGD retained in leg bones of OPG-treated animals 1, 2, and 24 h PI **c** Level of TRAP5b in sera from OPG-treated animals decreased significantly from the baseline while no change was observed in the control animals. Data are part of a biodistribution study with *n*=5 for each time point for treated and control groups.

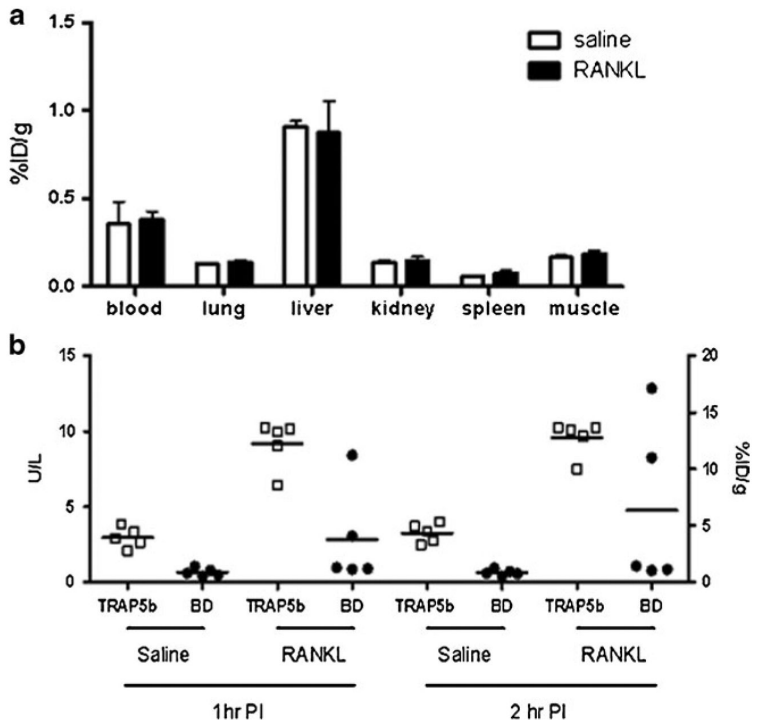

Fig. 3.

a ^{64}Cu-RGD uptake in non-osseous organs was similar between the treated and control groups (2 h PI shown). Averages of *n*=5 for each group at each time point are shown. **b** Correlation of serum TRAP5b data with%ID/g of ^{64}Cu-RGD in bone in mice treated with 0.3 mg/kg RANKL. The left axis corresponds to units per liter for serum TRAP5b, while the right axis corresponds to%ID/g of ^{64}Cu-RGD in bone. The data demonstrated a statistically significant increase in TRAP5b levels after treatment with RANKL and a positive correlation between TRAP5b levels and%ID/g of ^{64}Cu-RGD in bone.

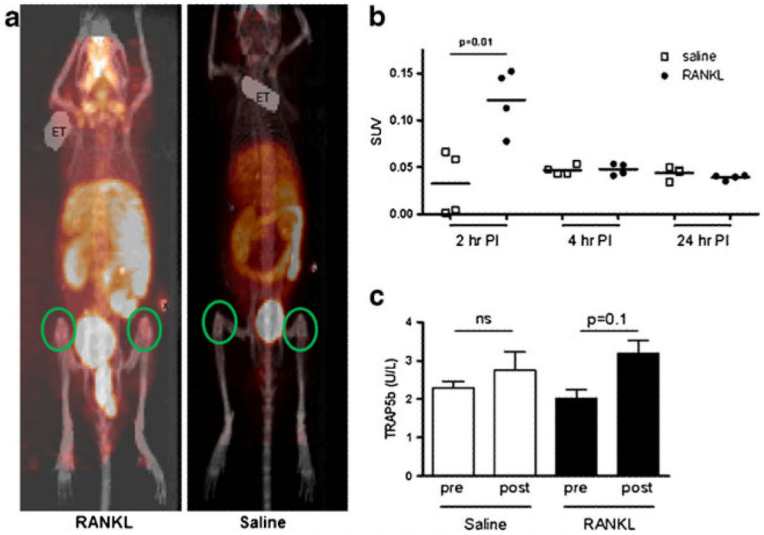

Fig. 4.

Standard uptake values (SUVs) of co-registered PET/CT image demonstrated significantly increased uptake of ^{64}Cu-RGD in leg bones of RANKL (0.3 mg/kg) treated animals (*n*=4 for each group). **a** Representative maximum intensity projection image of RANKL (L) and saline (R) treated animals. ROIs were drawn around knee joints (green circles). ET ear tags, X fiduciary marker. **b** Averaged leg bone SUV. **c** Serum levels of TRAP5b in RANKL- and saline-treated animals before and after treatment.

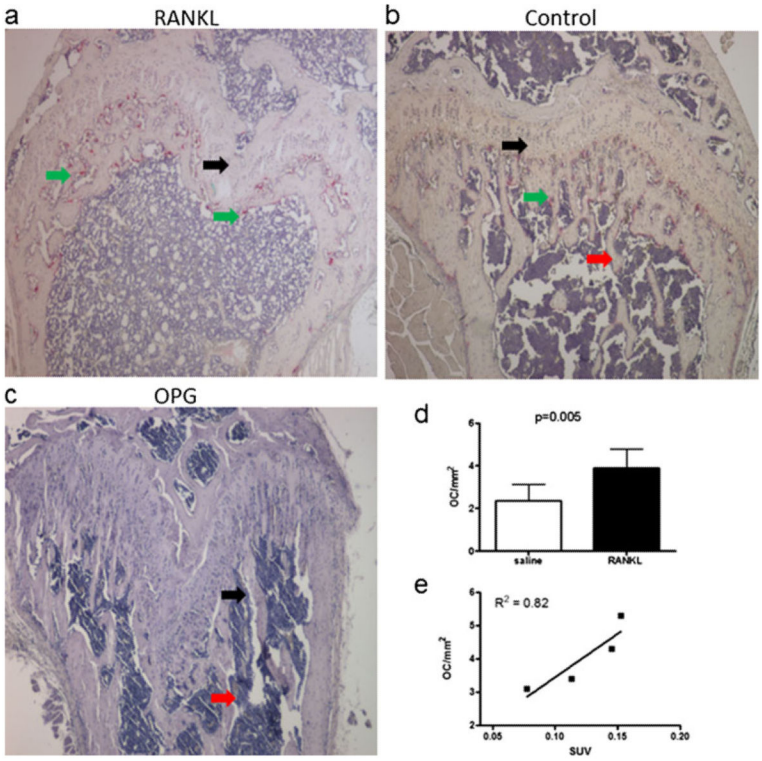

Fig. 5.

Histological analysis confirmed increased (RANKL) and decreased (OPG) number of osteoclasts in leg bones of study animals. **a** Histological sections of femurs from RANKL-, **b** saline-, and **c** OPG-treated mice. *Green arrows* osteoclasts. *Black arrows* growth plate. *Red arrows* trabecular bone. **d** Averaged number of osteoclasts per unit of area in leg bones of animals treated with RANKL or saline (n=5 for RANKL-treated animals, n=10 for control animals). **e** Correlation between the osteoclast surface area and the SUV of leg bones from small animal PET imaging studies. The R^2 of 0.82 demonstrates a strong correlation.